

Manipulating metal-insulator transitions of VO_2 films via embedding Ag nanonet arrays

Zhangyang Zhou(周章洋), Jia Yang(杨佳), Yi Liu(刘艺), Zhipeng Gao(高志鹏), Linhong Cao(曹林洪), Leiming Fang(房雷鸣), Hongliang He(贺红亮), and Zhengwei Xiong(熊政伟)

Citation: Chin. Phys. B, 2021, 30 (**12**): 126803. DOI: 10.1088/1674-1056/ac003a
Journal homepage: http://cpb.iphy.ac.cn; http://iopscience.iop.org/cpb

What follows is a list of articles you may be interested in

Probing thermal properties of vanadium dioxide thin films by time-domain thermoreflectance without metal film

Qing-Jian Lu(陆青鑑), Min Gao(高敏), Chang Lu(路畅), Fei Long(龙飞), Tai-Song Pan(潘泰松), and Yuan Lin(林媛)
Chin. Phys. B, 2021, 30 (**9**): 096801. DOI: 10.1088/1674-1056/abea94

The influence of surface effects on Frederiks transition in nematic liquid crystal doped with ferroelectric nanoparticles

Erfan Kadivar, Mojtaba Farrokhbin
Chin. Phys. B, 2018, 27 (**4**): 046801. DOI: 10.1088/1674-1056/27/4/046801

Gas adsorption and accumulation on hydrophobic surfaces: Molecular dynamics simulations

Luo Qing-Qun, Yang Jie-Ming
Chin. Phys. B, 2015, 24 (**9**): 096801. DOI: 10.1088/1674-1056/24/9/096801

Fabrication of VO_2 thin film by rapid thermal annealing in oxygen atmosphere and its metal-insulator phase transition properties

Liang Ji-Ran, Wu Mai-Jun, Hu Ming, Liu Jian, Zhu Nai-Wei, Xia Xiao-Xu, Chen Hong-Da
Chin. Phys. B, 2014, 23 (**7**): 076801. DOI: 10.1088/1674-1056/23/7/076801

Structural and optical properties of tungsten-doped vanadium dioxide films

Wang Xue-Jin, Liu Yu-Ying, Li De-Hua, Feng Bao-Hua, He Zhi-Wei, Qi Zheng
Chin. Phys. B, 2013, 22 (**6**): 066803. DOI: 10.1088/1674-1056/22/6/066803

Manipulating metal–insulator transitions of VO_2 films via embedding Ag nanonet arrays*

Zhangyang Zhou(周章洋)[1,2], Jia Yang(杨佳)[1], Yi Liu(刘艺)[1], Zhipeng Gao(高志鹏)[1,†], Linhong Cao(曹林洪)[4], Leiming Fang(房雷鸣)[3], Hongliang He(贺红亮)[1], and Zhengwei Xiong(熊政伟)[2,‡]

[1] *Institute of Fluid Physics, China Academy of Engineering Physics, Mianyang* 621900, *China*
[2] *Joint Laboratory for Extreme Conditions Matter Properties, Southwest University of Science and Technology, Mianyang* 621010, *China*
[3] *Institute of Physics, Nuclear, and Chemistry, China Academy of Engineering Physics, Mianyang* 621900, *China*
[4] *School of Materials Science and Engineering, Southwest University of Science and Technology, Mianyang* 621010, *China*

(Received 28 March 2021; revised manuscript received 8 May 2021; accepted manuscript online 12 May 2021)

Manipulating metal–insulator transitions in strongly correlated materials is of great importance in condensed matter physics, with implications for both fundamental science and technology. Vanadium dioxide (VO_2), as an ideal model system, is metallic at high temperatures and shown a typical metal–insulator structural phase transition at 341 K from rutile structure to monoclinic structure. This behavior has been absorbed tons of attention for years. However, how to control this phase transition is still challenging and little studied. Here we demonstrated that to control the Ag nanonet arrays (NAs) in monoclinic VO_2(M) could be effective to adjust this metal–insulator transition. With the increase of Ag NAs volume fraction by reducing the template spheres size, the transition temperature (T_c) decreased from 68 °C to 51 °C. The mechanism of T_c decrease was revealed as: the carrier density increases through the increase of Ag NAs volume fraction, and more free electrons injected into the VO_2 films induced greater absorption energy at the internal nanometal–semiconductor junction. These results supply a new strategy to control the metal–insulator transitions in VO_2, which must be instructive for the other strongly correlated materials and important for applications.

Keywords: vanadium dioxide, volume fraction, Ag nanonet arrays, metal–insulator transition

PACS: 68.03.–g, 68.35.–p **DOI:** 10.1088/1674-1056/ac003a

1. Introduction

Metal–insulator transition (MIT), which is one of the most attractive phenomena in transition metal oxides (TMOs),[1–4] can be driven by various parameters such as element doping, temperature, external pressure, photo-excitation, magnetic field, electric field, and so on.[5–13] The common signature of a phase transition is the sudden change of one or more thermodynamical variables.[9,10] One of emerging parameters of MIT is the control of switching T_c between the metal–insulator phases.[8] VO_2, as an ideal model system, is metallic at high temperatures and shown a typical metal–insulator structural phase transition at 341 K from rutile structure to monoclinic structure.[11] This dramatic MIT makes VO_2 potentially useful for 'smart' optical and electrical switches, which yet requires the regulation of T_c to around room temperature.[11–15] The mechanism of this MIT has been explained in various ways, such as, localization by the surface scattering, bandwidth narrowing due to the reduced dimensionality, strain, and so on.[15–17] In the past few decades, researchers have made great efforts to solve this problem.[11–18] The most effective route for appreciable reduction of T_c is doping some donor impurity atoms, which could be easily realized by chemical substitution methods, especially tungsten (W^{6+}) with dramatic reduction rates of 20 °C–28 °C per at.%.[7,14,19] The strong interaction between doped atoms and VO_2 lattices across the MIT induces the T_c reduction.[19] Another way to manipulate T_c is that metal nanoparticles are embedded into VO_2(M) matrix.[20–24] Due to the special local plasma resonance effects (LSPR) of noble metal nanoparticles (*e.g.* Au and Ag),[21–24] external photon injection brings the resonant absorption of energy, consequently reducing the T_c.[25–27] Until now, most research attached importance to the external stimulus of light for the T_c tuning,[26–28] considering that the MIT nature of metal nanoparticles/VO_2 system in a lightless environment has as yet received little study. In spite of its importance, however, the underlying physical mechanisms to drive MIT when metal nanoparticles are involved are not well understood. Researchers often study the intrinsic properties of materials in dark environments.[3,5] In view of this issue, it is highly meaningful to explore the MIT of metal nanoparticles/VO_2 system with a dark environment.

In this study, the Ag nanonet arrays was embedded in the VO_2(M) film by polystyrene (PS) template etching approach and electron-beam evaporation method. By changing the vol-

*Project supported by the National Natural Science Foundation of China (Grant Nos. 11904299 and U1930124) and the Foundation of China Academy of Engineering Physics (Grant No. 2018AB02).

†Corresponding author. E-mail: zhipenggao1020@163.com
‡Corresponding author. E-mail: zw-xiong@swust.edu.cn

© 2021 Chinese Physical Society and IOP Publishing Ltd

ume fraction of Ag nanoparticles in the composites, the phase transition temperature with a dark environment of composite films was studied.

2. Experimental details

2.1. Preparation of VO_2 films

The preparation methods of VO_2 films were reported previously.[23,29–31] In a high vacuum environment, the electron-beam evaporation system was used evaporate the VO_2 target to grown VO_2 films (base pressure 5.0×10^{-5} Pa, working pressure 5×10^{-3} Pa). Thin films with 200-nm nominal thickness were grown on quartz (SiO_2 15 mm × 15 mm) substrates heated at 300 °C (deposition rate ~ 0.5 nm·s^{-1}). The optimization of the growth process revealed that a subsequent *in-situ* annealing at 500 °C for 30 min under air atmosphere of 10-Pa pressure was necessary to obtain films with the desired quality.[23] Finally, pure VO_2(M) film was obtained and labeled as S_0 sample.

2.2. Etching PS templates

Close-packed monolayer PS templates were prepared via a modified interface assembly method (Figs. 1(a)–1(c)).[32,33] In brief, 0.3-wt% PS sphere dispersion in a 1:1 by volume mixture of deionized water:anhydrous ethanol was dropped slowly on the water/air interface by the drainage glass. Then several drops of sodium dodecyl benzene sulfonate (SDBS) solution (2 wt%) were added to push the floating PS spheres to form an iridescent film, followed by being picked up with SiO_2 substrates. Subsequently, the close-packed monolayer PS templates were rendered etched to be non-close-packed by a Plasma Pro 80 RIE (Oxford, England) Plasma Etch System performed used a mixture gas of argon and oxygen with 1:5 in pressure and an RF power of 100 W (Fig. 1(d)). The plasma etching duration was 0, 200, 400, and 500 s to obtain nanonet structures, respectively.

2.3. Preparation of Ag NAs/VO_2 composite films

The etched PS templates were placed in a vacuum chamber and evaporated Ag target for 20 min, as shown in Fig. 1(e). Then the PS templates plated with the Ag films were immersed in toluene, and the PS spheres were removed by ultrasound. The high-quality Ag NAs with variable periodicity were obtained (Fig. 1(f)). Finally, a VO_2 layer was covered on Ag NAs to obtain Ag NAs/VO_2 composite films (Fig. 1(g)).[23] Based on four etched PS templates (diameter = 1080, 862, 647, and 538 nm), the composite films with different Ag sizes were labeled as S_1, S_2, S_3, and S_4 samples, respectively.

2.4. Characterization

The surface morphology was characterized using field-emission scanning electron microscope (FE-SEM, Carl Zeiss Supra VP55, Germany) at an accelerating voltage of 10 kV. The crystal phases were identified by thin-film glancing incidence x-ray diffraction (GIXRD, X' pert Pro MPD, Netherlands) with Cu $K\alpha$ x-rays. The electrical switching behavior of the films was studied by using the four-probe system in dismal surroundings which was equipped with a Keithley 2400 (Tektronix, America) source meter. The carrier concentration of the samples was measured by Hall measurement system (Nanometrics HL5500PC, America), at room temperature.

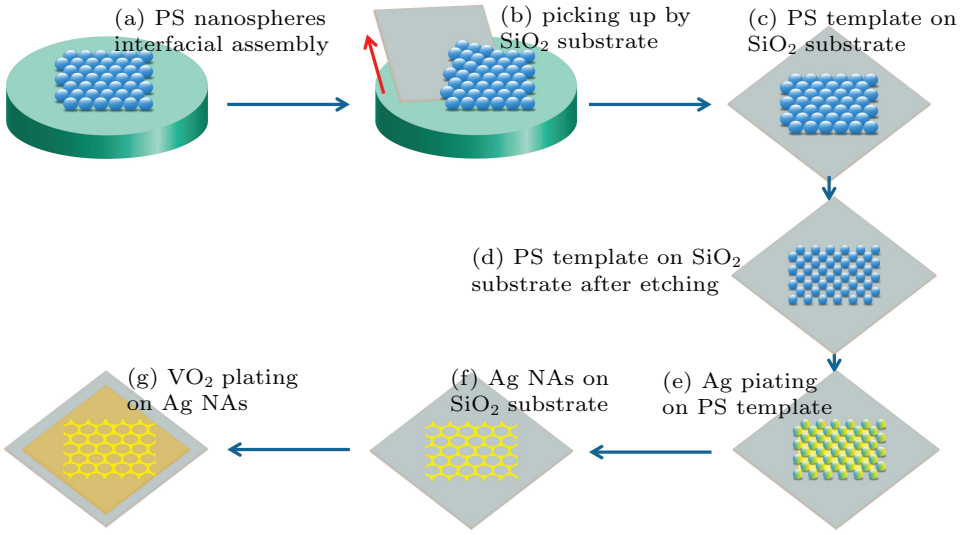


Fig. 1. Schematic diagram of the procedure to made Ag NAs/VO_2 composite films: [(a)–(c)] preparation of PS templates, (d) etching PS templates, and [(e) and (f)] fabrication of Ag NAs/VO_2 composite films.

3. Results and discussion

Figure 2 shows the GIXRD patterns of the samples measured at room temperature. As depicted, the samples grown at 300 °C exhibit one weak diffraction peak of $2\theta \approx 25.2°$, corresponding to the crystalline orientation of VO_2(B) (110) (space group $C2/m$, JCPDS File Card No. 81-2392).[34] Films an-

nealed at 500 °C exhibit strong peaks at $2\theta \approx 27.9°$, 37.1°, and 55.6° and are assigned to (011), ($\bar{2}$11), and (220) orientations of the VO_2(M) (space group $P2_1/c$, JCPDS File Card No. 65-2358).[14] Except for the VO_2(M), no other phase is detectable after annealing. The phase transformation from VO_2(B) to VO_2(M) is achieved by heating VO_2(B) at relatively high temperature to overcome the energy barrier to form the most thermodynamically stable phase VO_2(R), which again converts to VO_2(M) upon cooling below T_c.[34,35] After embedding Ag NAs, the film exhibited new strong peaks at $2\theta \approx 38.2°$, 44.4°, and 64.6°, assigned to (111), (200), and (220) orientations of Ag (space group Fm-3m, JCPDS File Card No. 87-0720).[35] A co-existence of both VO_2(M) and Ag phases without any impurities is displayed in the composites, revealing the well combination of the two materials.

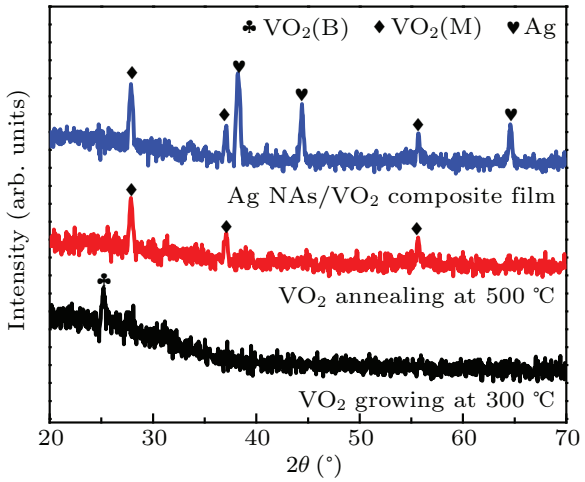


Fig. 2. GIXRD of the samples

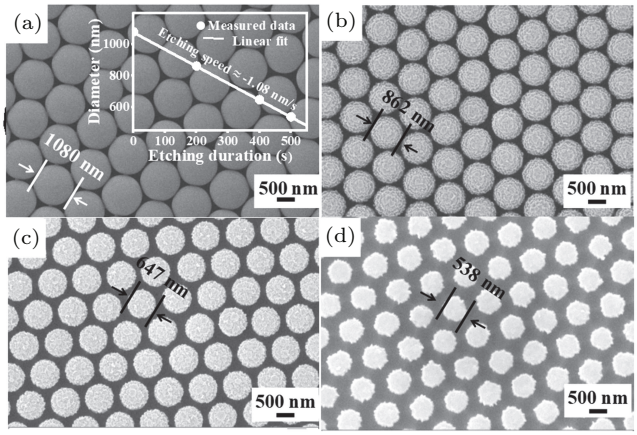


Fig. 3. [(a)–(d)] FESEM images of PS templates after Ar/O_2 plasma etching for 0, 200, 400, and 500 s, respectively. Inset of panel (a) is the linear relationship of PS sphere diameter and etching duration.

The PS template is a hexagonal close-packed monolayer supported on the SiO_2 substrate (Fig. 3(a)). The diameter of PS spheres particle is 1080 nm. The inter distance between two adjacent PS spheres is controlled via Ar/O_2 plasma etching. The average diameters of PS spheres are measured to be 862 (Fig. 3(b)), 647 (Fig. 3(c)), and 538 nm (Fig. 3(d)) after plasma etching duration of 200, 400, and 500 s, respectively. At the same time, the PS template still retains the spherical shape after etching, indicating that the etching process is isotropic.[36,37] The hexagonal close-packed structure remains and adheres well on SiO_2 substrate after the treatment. PS spheres are diminished uniformly and their patterned structures are preserved. The diameter of spheres decreases rectilinear with etching duration with a speed of $\sim$ 1.08 nm/s measured by SEM (inset of Fig. 3(a)). These characters combined with the high reproducibility demonstrate that the plasma etching method is the effective means to precisely control the size of the PS sphere in monolayer colloidal crystal templates.[1,38]

The interspace between the PS spheres is used as templates to produce size-controlled nanonet arrays. Different sizes of Ag NAs are generated by removing PS spheres.[18] As shown in Figs. 4(a)–4(d), the high-quality Ag NAs are prepared with variable periodicity, corresponding to PS templates with diameters of 1080, 862, 647, and 538 nm, respectively. Then VO_2(M) films were coated on the Ag NAs to form Ag NAs/VO_2(M) composites, as shown in Figs. 4(e)–4(h), corresponding to S_1, S_2, S_3, and S_4, respectively. For embedded Ag NAs, it can be approximately regarded as composed of numerous regular hexagons of equal size (regular hexagon marked in Fig. 4).[23] The length of side of the regular hexagon is equal to the diameter of the unetched PS template sphere (1080 nm). At the same time, the particle metrics of the embedded Ag nanonet can be geometrically defined by the corresponding PS templates.[23] In a regular hexagon, the area (S) in-plane of Ag particles can be estimated from the equation

$$S = 6\sqrt{3}R^2 - 3\pi r^2, \tag{1}$$

where R ($R = 540$ nm) is the radius of PS spheres before etching and r is after etching. The height of Ag particles ($h = 50$ nm) should be equal to the thickness of Ag films.[23,36] According to the in-plane area and out-of-plane height of Ag particles, the volume fraction (φ) of Ag particles in composite films can be given by

$$\phi = \frac{hS}{hS + 6\sqrt{3}HR^2}, \tag{2}$$

where H ($H = 200$ nm) is the thickness of the VO_2(M) films, and hS is the volume of Ag particles in a regular hexagon.

From formulas (1) and (2), the Ag volume fractions were obtained in Table 1. Obviously, as the particle radius of the PS template sphere decreases from 540 nm to 269 nm, the Ag particles volume and volume fraction of Ag particles increases. Therefore, Ag NAs with a controlled volume fractions were successfully embedded in the VO_2(M) films.

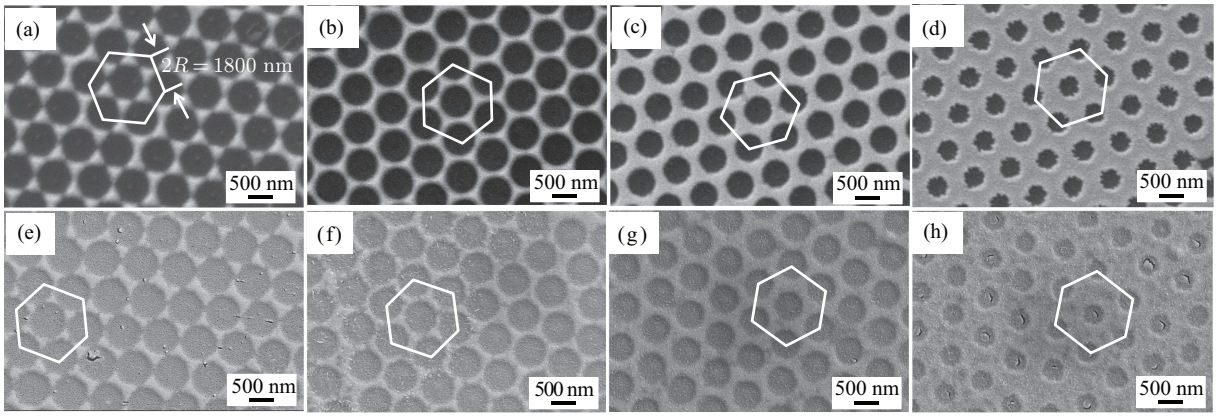


Fig. 4. [(a)–(d)] FESEM images of Ag NAs with different sizes, and [(e)–(h)] Ag NAs/VO_2(M) composites with different Ag volume fractions.

Table 1. Ag particles volume and volume fractions obtained from PS spheres at different plasma etching durations.

Sample	Etching duration (s)	r (nm)	hS (10^7 nm^3)	φ (100%)
S_1	0	540	1.41	2.27
S_2	200	431	6.40	9.55
S_3	400	323.5	10.22	14.43
S_4	500	269	11.74	16.23

Figure 5(a) shows the relationship between the resistivity and temperature of the samples in a dark environment. In each samples, the phase transition is observed along with the expected hysteresis during cooling.[23] Here, we focus on the the phase transition characteristics with increasing temperature. At room temperature, the samples show semiconductor characteristics and resistivity are about 0.2 Ω/cm–4 Ω/cm. The resistivity drops sharply at about 68 °C with the increase of temperature. A change of nearly two orders of magnitude in the resistivity of the films is observed in a smaller temperature range, indicates that MIT has occurred.[23] At the same time, it is also found that the amplitude of thermal hysteresis loop decreases as the embedded Ag volume fraction increases. These variations are attributed to Ag embedding introduced more free electrons, increases carrier concentration, and thus reduces the resistivity of the material.[39] The T_c value was considered to be the center of the thermal hysteresis loop.[22–24] The variation trend of T_c with Ag volume fraction is shown in Fig. 5(b) (red broken line). Obviously, the embedding of Ag NAs has a significant impact on T_c. As the Ag volume fraction increases, T_c decreases. More specifically, when the Ag volume fraction increased from 0 (S_0) to 16.23 % (S_4), T_c decreased from 68 °C to 51 °C. As shown in Fig. 5(b) (blue broken line), the carrier density increases as the embedded Ag NAs volume fraction increases. Specifically, the carrier density increases from 2.58×10^{18} cm^{-3} (S_0) to 54.63×10^{18} cm^{-3} (S_4) when the Ag volume fraction increased from 0 (S_0) to 16.23% (S_4). The measured carrier density of the pure VO_2(M) film is close to the result reported by Zhou *et al.*, indicating that the Hull measurement is valid.[40]

Previous studies had proved that VO_2(M) is an N-type semiconductor in which electrons play a leading role in the conduction mechanism.[23,40] So, with the embedded Ag volume fraction increases, the decreased T_c and increased carrier density are due to more free electrons injected into the VO_2(M) films.

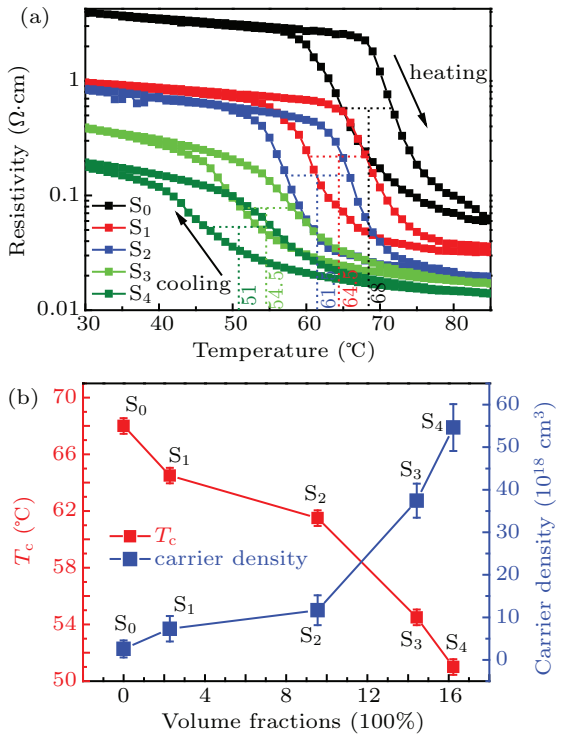


Fig. 5. (a) Resistivity–temperature curves of the samples, (b) temperature, carrier density–volume fractions relationship of the samples.

This phenomenon was actually confirmed in the 1975s.[41] The increase of free electrons concentration will lead to phase transition at a lower temperature.[23,41] In order to understand more clearly for this phenomenon, we used the changes of energy band with materials Ag and VO_2(M) before and after contact to explain, as shown in Fig. 6. As depicted in Fig. 6(a), the vacuum level E_0 as a reference. The work function W_m (4.6 eV)[42,43] of materials Ag is much lower than N-type VO_2(M) ($W_s = 5.4$ eV).[43,44] Ag and VO_2(M) contact

while formed an Ohmic junction,[23] which promotes the electrons transition from high (Ag) to low (VO_2(M)) concentration until their Fermi levels E_{Fm} and E_{Fs} align, and absorbed energy (W_A) at the junction, as shown in Fig. 6(b).[44,45] The absorbed energy is proportional to the number of electrons flowing into the semiconductor.[45] For the Ag/VO_2 system, the energy of phase transition is fixed, the energy provided by the heating system will decrease with the more energy is absorbed, corresponding to cut down T_c.[23] The mechanism of T_c reduction in Ag NAs/VO_2(M) composites: as the Ag volume fraction increases, more free electrons are injected into the VO_2(M) films to generate greater absorption energy at the nanometal–semiconductor junction, thus lowering T_c.

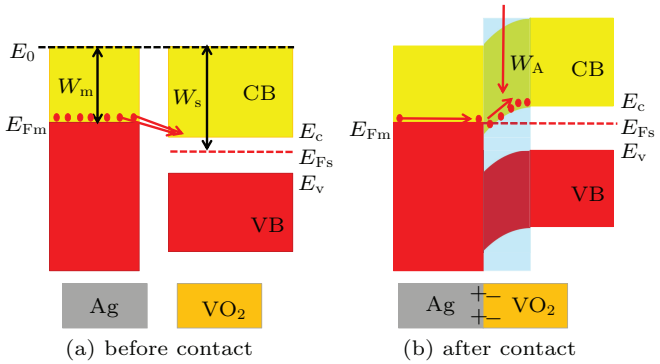


Fig. 6. Energy band of Ag/VO_2. The red solid spheres represent the excited electrons. E_0 is the vacuum level. E_{Fm} and E_{Fs} are the Fermi levels of Ag and VO_2, respectively. E_c and E_v are the conduction band (CB) and valence band (VB) of VO_2, respectively. W_m and W_s are work functions of Ag and VO_2, respectively. W_A is the energy absorbed in the contact region when electrons are injected from Ag to VO_2.

4. Conclusions

In this paper, we prepared the Ag NAs with controllable periodicity embedded into VO_2(M) films via nanosphere lithography. By adjusting the size of the PS nanospheres by changing the etching time, Ag NAs with different volume fractions were obtained in the Ag NAs/VO_2(M) composite films. On this based, it was found that T_c decreased from 68 °C to 51 °C, and the carrier density increased with the increased volume fraction. Combined with the energy-band analysis of Ag/VO_2(M), the detailed mechanism of T_c reduction was explained that more free electrons injected into the VO_2(M) films, the greater the energy absorbed at the nanometal–semiconductor junction.[23] These results provide a reference for controlling the metal–insulators transition in VO_2, and have directive significance for the application and development of other strongly correlated materials.

References

[1] Hong K, Moon C, Suh J, Lee T, Kim S, Lee S and Jang H 2019 *ACS Appl. Mater. Inter.* **11** 11568
[2] Trastoy J, Camjayi A, Valle J, Kalcheim Y and Schuller I K 2020 *Phys. Rev. B* **101** 245109
[3] Ramirez J G, Saerbeck T, Wang S, Trastoy J, Malnou M, Lesueur J, Crocombette J P, Villegas J E and Schuller I K 2015 *Phys. Rev. B* **91** 205123
[4] Wickramaratne D, Bernstein N and Mazin I I 2019 *Phys. Rev. B* **99** 214103
[5] Chen Y, Wang Z, Chen S, Ren H, Li B, Yan W, Zhang G, Jiang J and Zou C 2018 *Nano Energy* **51** 300
[6] Wang Z, Wang X, Sharman E, Li X, Yang L, Zhang G and Jiang J 2020 *J. Phys. Chem. Lett.* **11** 1075
[7] Matsuda Y H, Nakamura D, Ikeda A, Takeyama S, Suga Y, Nakahara H and Muraoka Y 2020 *Nat. Commun.* **11** 1842
[8] Duvjir G, Choi B K, Jang I, Ulstrup S, Kang S, Ly T T, Kim S, Choi Y H, Jozwiak C, Bostwick A, Rotenberg E, Park J, Sankar R, Kim K, Kim J and Chang Y J 2018 *Nano Lett.* **18** 5432
[9] Lu Q, Bishop S R, Lee D, Lee S, Bluhm H, Tuller H L, Lee H N and Yildiz B 2018 *Adv. Funct. Mater.* **28** 18030241
[10] Kim S Y, Lee M C, Han G, Kratochvilova M, Yun S, Moon S J, Sohn C, Park J G, Kim C and Noh T W 2018 *Adv. Mater.* **30** 17047771
[11] Huang T, Kang T, Li Y, Li J, Deng L and Bi L 2018 *Opt. Mater. Express* **8** 2300
[12] Miao L, Peng Y, Wang D, Liang J, Hu C, Nishibori E, Sun L, Fisher C A J and Tanemura S 2020 *Phys. Chem. Chem. Phys.* **22** 7984
[13] Lu W, Zhao G, Song B, Li J, Zhang X and Han G 2017 *Surf. Coat. Tech.* **320** 311
[14] Cui Y, Ke Y, Liu C, Chen Z, Wang N, Zhang L, Zhou Y, Wang S, Gao Y and Long Y 2018 *Joule* **2** 1707
[15] Alexander P, Andrey V, Maksim B and Vadim P 2018 *Phys. Rev. B* **536** 239
[16] Blagojevic V A, Obradovic N, Cvjeticanin N and Minic D M 2013 *Sci. Sinter.* **45** 305
[17] Hu B, Zhang Y, Chen W, Xu C and Wang Z 2011 *Adv. Mater.* **23** 3536
[18] Li M, Magdassi S, Gao Y and Long Y 2017 *Small* **13** 1701147
[19] Tian X, Wu C, Xie Y, Wei S, Yao T, Long R, Sun Z, Feng Y, Cheng H and Yuan X 2012 *Sci. Rep-UK* **2** 466
[20] Kim G H, Rathi S, Baik J M and Yi K S 2015 *Curr. Appl. Phys.* **15** 1107
[21] Li M, Ji S, Pan J, Wu H, Zhong L, Wang Q, Li F and Li G 2014 *J. Mater. Chem. A* **2** 48
[22] Lu X, Xiao X, Cao Z, Cheng H and Xu G 2016 *RSC Adv.* **6** 47249
[23] Zhou Z, Li J, Xiong Z, Cao L, Fu Y and Gao Z 2020 *Sol. Energy Mater. Sol. Cells* **206** 110303
[24] Zhou L, Hu M, Song X, Li P, Qiang X and Liang J 2018 *Appl. Phys. A* **124** 5051
[25] Ferrara D W, MacQuarrie E R, Diez-Blanco V, Nag J, Kaye A B and Jr R F H 2012 *Appl. Phys. A* **108** 255
[26] Madaras S E, Creeden J, Kittiwatanakul S, Lu J, Novikova I and Lukaszew R A 2018 *Opt. Express* **26** 25657
[27] Ferrara D W, Nag J, MacQuarrie E R, Kaye A B and Haglund R F Jr 2013 *Nano Lett.* **13** 4169
[28] Lysenko S, Rua A, Vikhnin V, Jimenez J, Fernandez F and Liu H 2006 *Appl. Surf. Sci.* **252** 5512
[29] Leroy J, Bessaudou A, Cosset F and Crunteanu A 2012 *Thin Solid Films* **520** 4823
[30] Thery V, Boulle A, Crunteanu A, Orlianges J C, Beaumont A, Mayet R, Mennai A, Cosset F, Bessaudou A and Fabert M 2016 *Phys. Rev. B* **93** 184106
[31] Vu T D, Chen Z, Zeng X, Jiang M, Liu S, Gao Y and Long Y 2019 *J. Mater. Chem. C* **7** 2121
[32] Xin Y, Jin H, Yong Z, Sun L, Feng G, Liu H, Wang F, Jiang X, Wu W and Zheng W 2017 *Nanomaterials* **7** 291
[33] Josh C, Choudhuri M, Raya M, Chowdhury D, Chattopadhyay P P and Datta A 2018 *Mater. Today* **5** 10143
[34] Popuri S R, Miclau M, Artemenko A, Labrugere C and Pollet M 2013 *Inorg. Chem.* **52** 4780
[35] Corr S A, Grossman M, Shi Y, Heier K R, Stucky G D and Seshadri R 2009 *J. Mater. Chem.* **19** 4362
[36] Grunwaldt J D, Atamny F, Gbel U and Baiker A 1996 *Appl. Surf. Sci.* **99** 353
[37] Ke Y, Wen X, Zhao D, Che R, Xiong Q and Long Y 2017 *ACS Nano* **11** 7542
[38] Hulteen J C and Richard P V D 1995 *J. Vac. Sci. Technol. A* **13** 1553
[39] Arndt A, Spoddig D, Esquinazi P, Barzola Q J, Dusari S and Butz T 2009 *Phys. Rev. B* **80** 195402
[40] Zhou Y and Ramanathan S 2013 *J. Appl. Phys.* **113** 213703
[41] Zylbersztejn A and Mott N F 1975 *Phys. Rev. B* **11** 4383
[42] Uda M, Nakamura A and Yamamoto T 1998 *J. Electron. Spectrosc.* **88** 643
[43] Chen L, Cui Y, Shi S, Luo H and Gao Y 2018 *Appl. Surf. Sci.* **450** 318
[44] Xu G, Huang C M, Tazawa M, Jin P, Chen D M and Miao L 2008 *Appl. Phys. Lett.* **93** 4383
[45] Takami H, Kanki T and Tanaka H 2016 *AIP Adv.* **6** 065118